Figure 1 ELISA indices and indirect immunofluorescence (IIF) titers before treatment and after remission. (a) ELISA indices of successfully treated BP patients. Disease remission was defined as when erythema, bullae and erosions had completely healed (complete remission) or no more than three bullae or erythema were seen in a week (partial remission) and only a low dose of oral prednisolone (<5 mg/d) or no treatment was needed to maintain this condition. As ELISA indices after remission, we adopted ELISA indices at the time when each patient's disease activity was evaluated as being in "complete remission" or "partial remission" (as defined above) for the first time after treatment. Mean ELISA index of the 10 patients before treatment was 91.3 ± 45.7 (range: 35.6–165.6) and the mean index after remission was 37.4 ± 25.3 (range: 6.0–86.4). After complete or partial remission, the ELISA indices were significantly reduced (P < 0.0001). (b) IIF titers of the same patients. Apparent decreases in IIF titers after remission were seen only in six patients. Mean IIF titer of the 10 patients before treatment was 201 ± 154 (range: 5–320) and the mean titer after remission was 60.5 ± 102.8 (range: 5–320). A statistically, significant reduction was observed in combined IIF titers after remission compared with those before treatment (P < 0.05). Colors of the lines are specific for each patient in both figures (a) and (b)

indices before treatment and after remission in our BP patient cohort and clearly demonstrated that ELISA indices significantly decreased after remission. Feng et al.[10] reported similar results on correlation of ELISA indices with disease course in BP patients, although the time points for ELISA after treatment were just before the decrease in corticosteroid and when the dosage of corticosteroid was successfully decreased to half the initial dose in the report. In this study, we employed ELISA indices at the time when each patient's disease activity was evaluated as "complete remission" or "partial remission" for the first time after treatment. Thus, this study is unique in the point that we evaluated exact correlation between ELISA indices and disease remission.

In conclusion, the present results further support the idea that the COL17 NC16A ELISA indices demonstrate a correlation with the BP disease remission more accurately than IIF titers and are a useful tool to detect BP disease remission and to assess the efficacy of BP treatment.

Erika Kusajima
Masashi Akiyama, MD, PhD
Megumi Sato
Ken Natsuga, MD
Hiroshi Shimizu, MD, PhD

Department of Dermatology
Hokkaido University Graduate School of Medicine
Sapporo
Japan
E-mail: akiyama@med.hokudai.ac.jp
Conflict of interest: the authors state no conflict of interest.

References
1 Giudice GJ, Emery DJ, Zelickson BD, et al. Bullous pemphigoid and herpes gestationis autoantibodies recognize a common non-collagenous site on the BP180 ectodomain. J Immunol 1993; 151: 5742–5750.
2 Zillikens D, Mascaro JM, Rose PA, et al. A highly sensitive enzyme-linked immunosorbent assay for the detection of circulating anti-BP180 autoantibodies in patients with bullous pemphigoid. J Invest Dermatol 1997; 109: 679–683.
3 Hata Y, Fujii Y, Tsunoda K, Amagai M. Production of the entire extracellular domain of BP180 (type XVII collagen) by baculovirus expression. J Dermatol Sci 2000; 23: 183–190.
4 Schmidt E, Obe K, Brocher EB, Zillikens D. Serum levels of autoantibodies to BP180 correlate with disease activity in patients with bullous pemphigoid. Arch Dermatol 2000; 136: 174–178.

5 Kobayashi M, Amagai M, Kuroda-Kinoshita K, *et al.* BP180 ELISA using bacterial recombinant NC16a protein as a diagnostic and monitoring tool for bullous pemphigoid. *J Deramtol Sci* 2002; 30: 224–232.

6 Tsuji-Abe Y, Akiyama M, Yamanaka Y, *et al.* Correlation of clinical severity and ELISA indices for the NC16A domain of BP180 measured using BP180 ELISA kit in bullous pemphigoid. *J Dermatol Sci* 2005; 37: 145–149.

7 Beutner EH, Jordon RE, Chorzelski TP. The immunopathology of pemphigus and bullous pemphigoid. *J Invest Dermatol* 1968; 51: 63–80.

8 Di Zenzo G, Thoma-Uszynski S, Fontao L, *et al.* Multicenter prospective study of the humoral autoimmune response in bullous pemphigoid. *Clin Immunol* 2008; 128: 415–426.

9 Izumi T, Ichiki Y, Esaki C, Kitajima Y. Monitoring of ELISA for anti-BP180 antibodies: clinical and therapeutic analysis of steroid-treated patients with bullous pemphigoid. *J Dermatol* 2004; 31: 383–391.

10 Feng S, Wu Q, Jin P, *et al.* Serum levels of autoantibodies to BP180 correlate with disease activity in patients with bullous pemphigoid. *Int J Dermatol* 2008; 47: 225–228.

prednisolone in HIV-infected individuals. J Acquir Immune Defic Syndr 2008;48:561-6.

5. Dort K, Padia S, Wispelwey B, Moore CC. Adrenal suppression due to an interaction between ritonavir and injected triamcinolone: a case report. AIDS Res Ther 2009;6:10.

Subepidermal blistering disease with 3 distinct autoantibodies: Anti-BP230, anti-laminin gamma-1, and anti-laminin-332

To the Editor: A 25-year-old Japanese woman presented with pruritic tense blisters involving the lips, forearms, fingers, and soles (Fig 1, *A-C*). No mucosal involvement was observed. A skin biopsy specimen taken from a bulla on her left forearm demonstrated subepidermal separation with eosinophilic inflammatory infiltrate in the dermis (Fig 2, *A*). Direct immunofluorescence (IF) microscopy of the lesion showed linear deposition of C3 and IgG at the dermoepidermal junction (Fig 2, *B* and *C*). Indirect IF on sodium-split skin revealed linear IgG deposition on both the epidermal and the dermal sides (titer 1:20; Fig 2, *D*). Enzyme-linked immunosorbent assay (ELISA) using bacterial recombinant protein of the NC16a domain of COL17 (MBL, Nagoya, Japan) was negative. ELISA using bacterial recombinant proteins of the N- and C-terminal domains of BP230 (MBL, Nagoya, Japan) was also negative. Immunoblot analysis with epidermal and dermal extracts derived from normal human skin and purified laminin-332 was performed. The results showed the presence of circulating IgG autoantibodies against BP230, laminin $\gamma 1$, and the $\gamma 2$ chain of laminin-332 (Fig 2, *E, F,* and *G*). Oral prednisolone, 40 mg per day (PSL), failed to alleviate the symptoms. With the addition of 75 mg per day of oral diaphenylsulfone (DDS), the cutaneous lesions rapidly healed with postinflammatory hyperpigmentation. PSL and DDS were tapered without relapse of skin lesions. At 10 months after referral, she discontinued PSL and was taking DDS at 25 mg daily.

Previously, antibodies against laminin-332 were detected in about 10% to 20% of mucous membrane pemphigoid (MMP) patients. The majority of the patients have antibodies reactive with the $\alpha 3$ subunit of the protein. However, our case showed reactivity only with the $\gamma 2$ subunit. The mucosal involvement that is typically seen in MMP was not observed in our case.

Circulating antibodies against BP230 were detected in the serum of a patient by immunoblot analysis but not by BP230 ELISA (MBL, Nagoya, Japan). This ELISA system utilizes the N- and C-terminal domains of BP230, but not the central-rod domain.[1] Therefore the autoantibodies against BP230
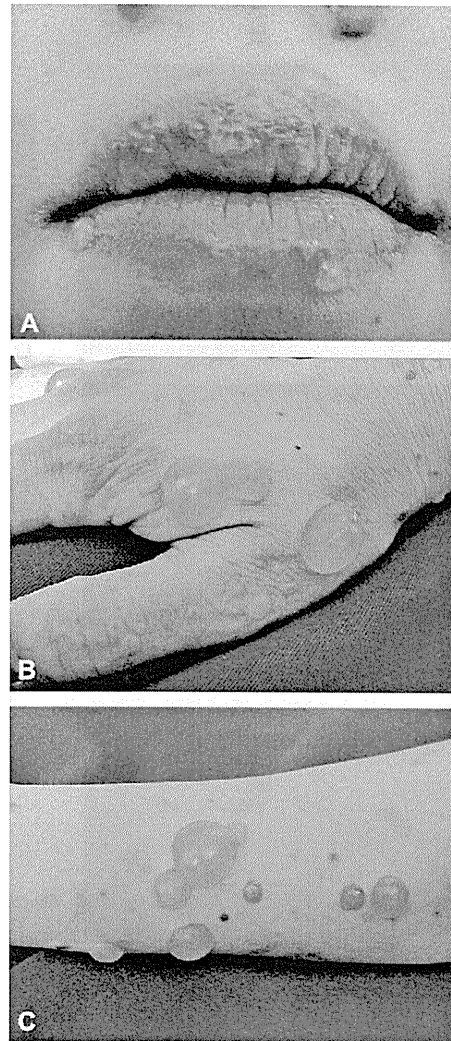

Fig 1. Clinical presentation of the patient. Tense blisters involve the fingers (**A**), forearms (**B**), and lips (**C**).

that were detected in our immunoblot study may have reacted with the central-rod domain of the BP230 antigen. Autoantibodies against BP230, an intracellular protein, are clearly associated with bullous pemphigoid (BP), but have not been shown to be involved in the initiation of the disease. A marked improvement with the administration of DDS and the absence of erythematous plaques in the patient were not typical of the BP clinical course and manifestations.

Autoantibodies against laminin $\gamma 1$ are characteristic of anti-laminin $\gamma 1$ pemphigoid.[2] Blisters involving the lips and therapeutic improvement with DDS are compatible with the clinical features of anti-laminin $\gamma 1$ pemphigoid. On the basis of these findings, the diagnosis of anti-laminin $\gamma 1$ pemphigoid may be appropriate.

It is possible that the unusual autoimmune profile of the patient developed as a result of epitope
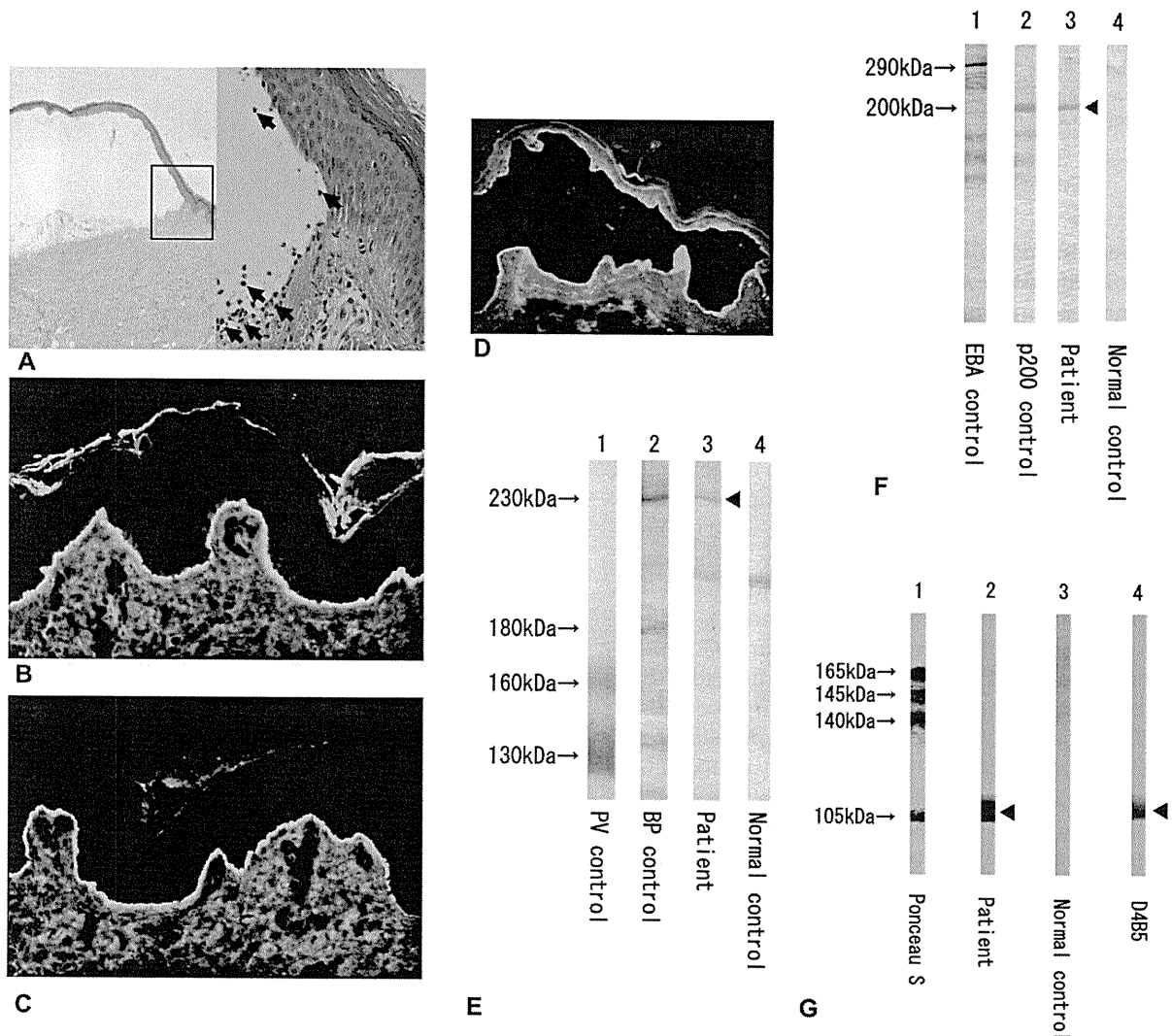
Fig 2. Histologic examination of skin specimens from patient's left forearm. **A**, Hematoxylin-eosin stain. Subepidermal blister (original magnification: ×40) with infiltration of eosinophils (*arrows*) in blister cavity (×200). Direct immunofluorescence of perilesional skin samples shows linear deposition of C3 (**B**) and IgG (**C**) at the dermoepidermal junction (×40). Immunological characterization of autoantibodies. **D**, Indirect immunofluorescence on 1M NaCl-split skin. Circulating IgG antibodies bind to both epidermal and dermal sides (titer 1:20). **E**, Immunoblot analysis using human epidermal extracts. *Lane 1*: A reference BP serum reacting with 180-kd (COL17) and 230-kd (BP230) antigens. *Lane 2*: A reference pemphigus vulgaris serum with positive bands at 130 kd (Dsg3) and 160 kd (Dsg1). *Lane 3*: Patient's serum. IgG in patient's serum reacts with BP230. **F**, Immunoblot analysis using human dermal extracts. *Lane 1*: A reference EBA serum reacting with a 290-kd molecule (type VII collagen). *Lane 2*: A reference anti-laminin γ1 pemphigoid serum with a positive band at 200 kd (p200, laminin γ1). *Lane 3*: Patient's serum. *Lane 4*: A reference normal serum. IgG in patient's serum reacts with 200-kd antigen. **G**, Immunoblot analysis using purified laminin-332 (courtesy of Dr S. Amano, Shiseido Life Science Research Center, Yokohama, Japan). *Lane 1*: A reference of Ponceau S stain of laminin-332 consisting of α3 (165 kd, 145 kd), β3 (140 kd), and γ2 (105 kd) subunits. *Lane 2*: Patient's serum. *Lane 3*: A reference normal serum. *Lane 4*: A reference of D4B5 (Millipore, Bedford, MA), a mouse monoclonal antibody against the γ2 subunit of laminin-332. IgG from patient's serum and D4B5 reacts with the γ2 subunit of laminin-332 (105 kd).

spreading. Although several cases of autoimmune blistering disease with distinct autoantigens have been reported,[3-5] to our knowledge this is the first case report describing a patient with IgG autoantibodies for three different antigens to the basement membrane zone: BP230, laminin γ1 and the γ2 subunit of laminin-332.

Kazuhiro Kikuchi, MD, PhD,[a,b] Ken Natsuga, MD, PhD,[b] Satoru Shinkuma, MD,[b] Wataru Nishie, MD, PhD,[b] Satoshi Kajita, MD, PhD,[c] Hidetsugu Sato, MD, PhD,[a] and Hiroshi Shimizu, MD, PhD[b]

Department of Dermatology, Obihiro Kosei General Hospital, Obihiro[a]; Department of Dermatology, Hokkaido University Graduate School of Medicine, Sapporo[b]; and Takagi Dermatology Clinic, Obihiro,[c] Japan

REFERENCES

1. Yoshida M, Hamada T, Amagai M, Hashimoto K, Uehara R, Yamaguchi K, et al. Enzyme-linked immunosorbent assay using bacterial recombinant proteins of human BP230 as a diagnostic tool for bullous pemphigoid. J Dermatol Sci 2006;41:21-30.
2. Dainichi T, Kurono S, Ohyama B, Ishii N, Sanzen N, Hayashi M, et al. Anti-laminin gamma-1 pemphigoid. Proc Natl Acad Sci U S A 2009;106:2800-5.
3. Izumi R, Fujimoto M, Yazawa N, Nakashima H, Asashima N, Watanabe R, et al. Bullous pemphigoid positive for anti-BP180 and anti-laminin 5 antibodies in a patient with graft-vs-host disease. J Am Acad Dermatol 2007;56:94-7.
4. Shimanovich I, Petersen EE, Weyers W, Sitaru C, Zillikens D. Subepidermal blistering disease with autoantibodies to both the p200 autoantigen and the alpha3 chain of laminin 5. J Am Acad Dermatol 2005;52:90-2.
5. Mitsuya J, Hara H, Ito K, Ishii N, Hashimoto T, Terui T. Metastatic ovarian carcinoma-associated subepidermal blistering disease with autoantibodies to both the p200 dermal antigen and the gamma 2 subunit of laminin 5 showing unusual clinical features. Br J Dermatol 2008;158:1354-7.

Thrombosis-induced ulcerations of the lower legs with coexistent anetoderma due to anti-thrombin III deficiency

To the Editor: A 54-year-old white man with schizoaffective disorder and insulin-dependent diabetes

Fig 1. Lesions of anetoderma surrounding thrombotic-induced ulceration on right leg.

mellitus presented with a several-month history of nonhealing, painful ulcerations of the lower extremities. On examination, the right lower extremity had a 10- × 6-cm ulcer with irregular borders. Closer observation revealed numerous flesh-colored, atrophic 1- to 2-cm plaques on skin surrounding the ulceration consistent with anetoderma (Fig 1). These lesions were asymptomatic and began concomitantly with ulcer development. Livedo reticularis was not present. Initial evaluation included a biopsy of the ulceration and laboratory investigation for hereditary and acquired hypercoagulable states. Histologic evaluation of the ulceration revealed deep and superficial thromboses with prominent overlying infarct, without evidence of primary vasculitis or pyoderma gangrenosum. Laboratory evaluation for anti-phospholipid antibodies and cryoglobulins were negative; however, anti-thrombin III activity was reduced. Repeat testing revealed below normal antithrombin III activity (mean, 74%; normal, 80%-120%) and reduced antigen level at 19.6% (normal, 22%-36%). A Doppler ultrasound of the lower extremities was negative for deep vein thrombosis.

The patient was referred to the hematology service; a trial of coagulation prophylaxis with enoxaparin (Lovenox, Sanofi-Aventis), 40 mg administered subcutaneously twice daily, was performed. This resulted in complete resolution of all skin lesions over several weeks (Fig 2). Several weeks later, the patient presented with recurrence of lower extremity ulcerations. It was discovered that the patient had self-discontinued treatment with enoxaparin because of pain with medication injection as well as cutaneous bleeding and bruising with minimal trauma. Subsequent replacement with fondaparinux (Arixtra, Glasko Smith Kline, Brentford,

Recurrence of Hydroxyurea-induced Leg Ulcer After Discontinuation of Treatment

Kazuhiro Kikuchi[1], Ken Arita[1], Yasuki Tateishi[1], Masahiro Onozawa[2], Masashi Akiyama[1] and Hiroshi Shimizu[1]
*Departments of [1]Dermatology and [2]Hematology, Hokkaido University Graduate School of Medicine, North 15 West 7, Kita-ku, Sapporo 060-8638, Japan.
E-mail: kikku@med.hokudai.ac.jp*

Hydroxyurea (HU) is a hydroxylated derivative of urea that has been recognized since 1960 as effective against cancer (1). It is an inhibitor of cellular DNA synthesis, and it promotes cell death in the S phase of the cell cycle through inhibition of the enzyme ribonucleotide reductase (2). The most common indications for HU therapy are chronic myeloid leukaemia and other myeloproliferative disorders (3, 4) such as essential thrombocythemia (5) and polycythemia vera (PV) (6). Cutaneous side-effects, such as alopecia, diffuse hyperpigmentation, scaling, lichen planus-like lesions, poikiloderma, atrophy of the skin and subcutaneous tissues, and nail changes, can occur during the treatment with HU (7–9). The occurrence of painful leg ulcers represents another rare and incompletely characterized complication that has been described in patients with myeloproliferative diseases receiving high-dose long-term HU treatment (10). While the mode of action of HU on bone marrow elements is well established, its effects on actively proliferating epithelial cells remain less described (11). Poor response to traditional local and systemic therapy is a typical feature of HU-induced leg ulcers, and discontinuation of the drug is often required to achieve complete wound healing (6, 8). Cessation of the drug usually improves the skin ulcer; although, in some cases, the ulcer remains and additional therapies, such as skin grafting, are needed (12). We report here the first case of a leg ulcer that recurred even after discontinuation of HU treatment.

CASE REPORT

The patient was an 82-year-old Japanese male who had been diagnosed with PV 9 years before and had been treated only with phlebotomy and an anti-platelet agent for several years. Due to splenomegaly and elevated blood cell counts, HU therapy was started 3 years ago at a dosage of 1 g daily for a month, followed by 1.0 or 1.5 g daily for 28 months. A good clinical response was achieved. However, the patient developed painful ulcers on the left second toe after two years of HU treatment.

He visited our outpatient clinic and was diagnosed with an HU-induced skin ulcer. HU was discontinued, topical application of sulfadiazine silver was performed, an oral antibiotic (cefdinir) was administered, and the ulcer epithelialized. However, a new ulcer appeared on the left lateral malleolar area 46 days after cessation of HU and gradually enlarged in size. The patient was admitted to our hospital for treatment of the ulcer.

Examination revealed a 48 × 56 mm ulcer with yellow necrotic tissue and marginal erythematous oedema (Fig. 1). Laboratory examination revealed a white blood cell count of $11.6 \times 10^3/\mu l$, a platelet count of $64.2 \times 10^4/l$, and a red blood cell count of $5.07 \times 10^6/\mu l$. Anti-nuclear antibody, anti-neutrophilic cytoplasmic antibodies, anti-cardiolipin antibody, and cryoglobulin were negative. A skin biopsy taken from the margin of the ulcer demonstrated leukocytoclastic vasculitis in the upper dermis (Fig. 2). A wound-healing strategy of surgical debridement, intravenous prostaglandin E1 administration, and topical application of beta-fibroblast growth factor, sulfadiazine silver and alprostadil alfadex was started, and the ulcer began to epithelialize. After 4 months, re-epithelialization was complete. The PV was treated with busulfan, achieving a good clinical response.

DISCUSSION

HU is usually well tolerated and has low toxicity (1). However, cutaneous adverse effects such as diffuse hyperpigmentation, brown discoloration of the nails, acral erythema, photosensitization, fixed drug eruption, alopecia, and oral ulceration have been reported (7–9). Stahl & Silber (10) first reported HU-induced skin ulcers in 1985. Montefusco et al. (11) reported

Fig. 1. Left foot with an ulcer on the lateral malleolar area after two months free of hydroxyurea administration. The ulcer was covered with yellow necrotic tissue and surrounded by oedematous erythema.
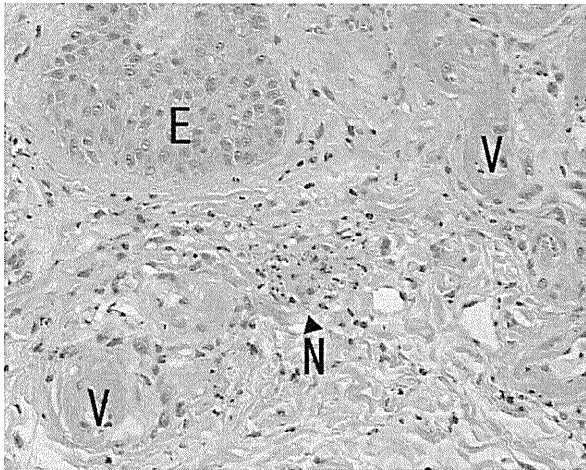
Fig. 2. Histology of erythema on the margin of the ulcer (haematoxylin-eosin staining). Fibrin deposition on the vascular wall and nucleic debris were evident around small vessels (×100). (E: epidermis; V: blood vessels; N: neutrophilic nuclear debris).

that, among 200 chronic myeloid leukaemia patients treated with HU, 17 (8.5%) developed leg ulcers. However, they achieved complete resolution or significant improvement after discontinuation of HU therapy (11). HU-induced leg ulcer and complete resolution within several months after drug discontinuation has also been reported in other myeloproliferative disorder, such as PV (6) and essential thrombocythemia (5). In those cases, as in ours, most of the patients had been treated with > 1 g of HU per day for at least one year (8). In the present case, the patient was treated with > 1 g of HU per day for 28 months. The ulcer occurred on his lateral malleolus, which histologically showed leukocytoclastic vasculitis. These features are consistent with previous reports of HU-induced leg ulcer.

From previous reports, the pathogenesis of HU-induced ulceration remains unclear and it may be multifactorial. It has been postulated that ulcers may be the result of: (*i*) interruption of microcirculation due to leukocytoclastic vasculitis or arterial microthrombi related to platelet dysregulation (13, 14); (*ii*) cumulative toxicity in the basal layer of the epidermis through inhibition of DNA synthesis (8); and (*iii*) repeated mechanical injury in areas subject to trauma: a perimalleolar area for instance (15).

In the case described here, a new ulcer developed even after cessation of HU administration. As for the pathogenic mechanism of recurrence, (*i*) interruption of microcirculation could result from hyperviscosity due to the elevated platelet count (as high as 100×10^4/l in one measurement) (13, 14), although no thrombi were observed histologically in the capillaries or small vessels. (*ii*) The direct cytotoxic effect of HU (8) may

continue even after the withdrawal of the drug, and it may inhibit the repair of (*iii*) small injuries in the perimalleolar area: the one of the area susceptible to physical trauma (15). These assumptions can be made from the pathogenesis of HU-induced ulcer reported previously (8, 13–15).

To our knowledge, this is the first report of recurrence of HU-related leg ulcer after the discontinuation of medication. The case suggests that it is important to pay careful attention to recurrence even after cessation of HU therapy. Precise, early treatment for microtraumas and small ulcers should be administered to patients with a long history of HU medication.

REFERENCES

1. Boyd AS, Neldner KH. Hydroxyurea therapy. J Am Acad Dermatol 1991; 25: 518–524.
2. Yarbro JW. Mechanism of action of hydroxyurea. Semin Oncol 1992; 19: 1–10.
3. Goldman JM. Therapeutic strategies for chronic myeloid leukemia in the chronic (stable) phase. Semin Hematol 2003; 40: 10–17.
4. Rice L, Baker KR. Current management of the myeloproliferative disorders: a case-based review. Arch Pathol Lab Med 2006; 130: 1151–1156.
5. Demirçay Z, Cömert A, Adigüzel C. Leg ulcers and hydroxyurea: report of three cases with essential thrombocythemia. Int J Dermatol 2002; 41: 872–874.
6. Bader U, Banyai M, Böni R, Burg G, Hafner J. Leg ulcers in patients with myeloproliferative disorders: disease- or treatment-related? Dermatology 2000; 200: 45–48.
7. Najean Y, Rain JD. Treatment of polycythemia vera: the use of hydroxyurea and pipobroman in 292 patients under the age of 65 years. Blood 1997; 90: 3370–3377.
8. Weinlich G, Schuler G, Greil R, Kofler H, Fritsch P. Leg ulcers associated with long-term hydroxyurea therapy. J Am Acad Dermatol 1998; 39: 372–374.
9. Daoud MS, Gibson LE, Pittelkow MR. Hydroxyurea dermopathy: a unique lichenoid eruption complicating long-term therapy with hydroxyurea. J Am Acad Dermatol 1997; 36: 178–182.
10. Stahl RL, Silber R. Vasculitic leg ulcers in chronic myelogenous leukemia. Am J Hematol 1985; 78: 869–872.
11. Montefusco E, Alimena G, Gastaldi R, Carlesimo OA, Valesini G, Mandelli F. Unusual dermatologic toxicity of long-term therapy with hydroxyurea in chronic myelogenous leukaemia. Tumori 1986; 72: 317–321.
12. Kato N, Kimura K, Yasukawa K, Yoshida K. Hydroxyurea-related leg ulcers in a patient with chronic myelogenous leukemia: a case report and review of the literature. J Dermatol 1999; 26: 56–62.
13. Sirieix ME, Debure C, Baudot N, Dubertret L, Roux ME, Morel P, et al. Leg ulcers and hydroxyurea: forty-one cases. Arch Dermatol 1999; 135: 818–820.
14. Chaine B, Neonato MG, Girot R, Aractingi S. Cutaneous adverse reactions to hydroxyurea in patients with sickle cell disease. Arch Dermatol 2001; 137: 467–470.
15. Saravu K, Velappan P, Lakshmi N, Shastry BA, Thomas J. Hydroxyurea induced perimalleolar ulcers. J Korean Med Sci 2006; 21: 177–179.

Spontaneous Remission of Solitary-Type Infantile Myofibromatosis

Kazuhiro Kikuchi[a] Riichiro Abe[a] Satoru Shinkuma[a]

Erika Hamasaka[a] Ken Natsuga[a] Hiroo Hata[a]

Yasuki Tateishi[a] Masahiko Shibata[a] Yuki Tomita[a]

Yukiko Abe[a] Satoru Aoyagi[a] Makio Mukai[b]

Hiroshi Shimizu[a]

[a]Department of Dermatology, Hokkaido University Graduate School of Medicine, Sapporo, and [b]Department of Pathology, Keio University School of Medicine, Tokyo, Japan

Key Words

Infantile myofibromatosis · Leiomyosarcoma · Solitary type

Abstract

Infantile myofibromatosis is a rare fibrous tumor of infancy. The cutaneous solitary type has typically an excellent prognosis. However, histologically, it is important to rule out leiomyosarcoma, which has a poor prognosis. The low frequency of mitosis was definitive for a diagnosis of infantile myofibromatosis. We present a cutaneous solitary-type case of infantile myofibromatosis. Following incisional biopsy, the tumor remitted spontaneously.

Introduction

Infantile myofibromatosis is a benign fibrous tumor of infancy and was first described by Stout in 1954 [1]. In most cases, it is present at birth, and in 90% of cases, the tumor appears within the first 2 years of life [2, 3]. The prognosis is excellent in the solitary type, which is limited in the skin, muscle, and subcutaneous lesions [2–4]. In contrast, the multicentric form of infantile myofibromatosis, which has visceral involvement, can be life-threatening [4, 5]. The solitary type is usually benign and the recurrence rate is low at 10%. Therefore, surgical excision is recommended [2, 6].

Kazuhiro Kikuchi, MD, PhD   Department of Dermatology
Hokkaido University Graduate School of Medicine, N15 W7, Kita-ku
Sapporo 060-8638 (Japan)
Tel. +81 11 716 1161, E-Mail kikku@med.hokudai.ac.jp

We present a case of a 3-week-old girl showing features of infantile myofibromatosis (solitary type). Excision was performed and no recurrence was detected in 24 months' follow-up.

Case Report

A 3-week-old, otherwise healthy Japanese girl had a solid, red-colored, cutaneous nodule on left shoulder. The nodule had a central concavity with a crust on the surface and measured 20 × 21 mm in diameter (fig. 1).

Physical examination and CT imaging of the head, chest, abdomen and pelvis revealed no additional lesions. No infiltration of the tumor into the muscle was identified by MRI imaging (fig. 2). Incisional biopsy was performed when the patient was 4 months old. The specimen showed multifocal sclerotic dermal nodules. The nodules were composed of spindle cells with round or oval nuclei and eosinophilic cytoplasm. Delicate bundles of eosinophilic fibers separated the cellular aggregates (fig. 3a, b). A diagnosis of infantile myofibromatosis, leiomyoma, leiomyosarcoma, histiocytoma, or other sarcoma was suggested. Spindle cells expressed smooth muscle actin (fig. 3c), but not caldesmon, desmin or S100 protein (not shown). The mitotic figures were very infrequent [6 mitoses per 10 low-power images (40×)]. These results were confirmed to be consistent with infantile myofibromatosis. The tumor gradually regressed until it completely disappeared 24 months after biopsy.

Discussion

Infantile myofibromatosis usually develops at birth or during the first years of life. Chung and Enzinger found the median age at presentation to be 3 months [2]. A slight male predominance among patients with both the solitary and multicentric variants was noted by Wiswell et al. [7]. Most cases of infantile myofibromatosis are solitary nodules, accounting for up to 70% of cases in one study [2], and up to 80% in another series [4]. The prognosis is excellent in the solitary type [2–4]. In the case of solitary-type infantile myofibromatosis, spontaneous regression can be expected [3, 4]. In contrast, a quarter of the cases with the multicentric form may have visceral involvement and can be life-threatening [2, 4, 5]. The solitary type of infantile myofibromatosis is usually benign and is typically found in the dermis, subcutis, or deep soft tissues. The distribution is predominantly on the head, neck, and trunk like our case. Involvement of the extremities is reported to be rare [2]. Solitary infantile myofibromatosis on an upper extremity accounted for only 13.3% in one study of 45 cases [8].

The histologic hallmark of infantile myofibromatosis is an un-encapsulated, well-circumscribed lobule of peripheral spindle cells, which bear a close resemblance to smooth muscle [9, 10]. Often there is a central area of hemangiopericytoma-like small rounded cells surrounding blood vessels [11, 12]. This combination of features gives infantile myofibromatosis its recognizable biphasic appearance, though the hemangiopericytoma-like appearance was not detected in this case. The presence of smooth muscle actin in the spindle cells indicates the diagnosis of infantile myofibromatosis or leiomyosarcoma. Considering the difference in prognosis, it was necessary to rule out leiomyosarcoma [13] in this case. While at least 1 mitotic cell per field in high-power (×200 or ×400) fields is detected in leiomyosarcoma [14], very infrequent mitotic figures [6 mitotic cells per 10 low-power (×40) fields] were observed, which definitively indicated infantile myofibromatosis in this case.

Previously, radical excision had been advocated as the treatment of choice, because it had been believed that the solitary form gave rise to multiple nodules with potential visceral involvement by metastases [15]. However, it is now more probable that the solitary and multicentric forms are distinct entities and that the solitary form remains localized and can regress [15]. Therefore, a wait-and-see approach has been suggested more recently as a treatment option [15]. However, in our patient, the decision was ultimately made to treat with surgical removal to exclude a diagnosis of leiomyosarcoma, which would have had a poor prognosis. The nodule disappeared completely after excision. The course was consistent with previous reports of solitary-type infantile myofibromatosis [2, 4, 15], and supports our histological diagnosis.
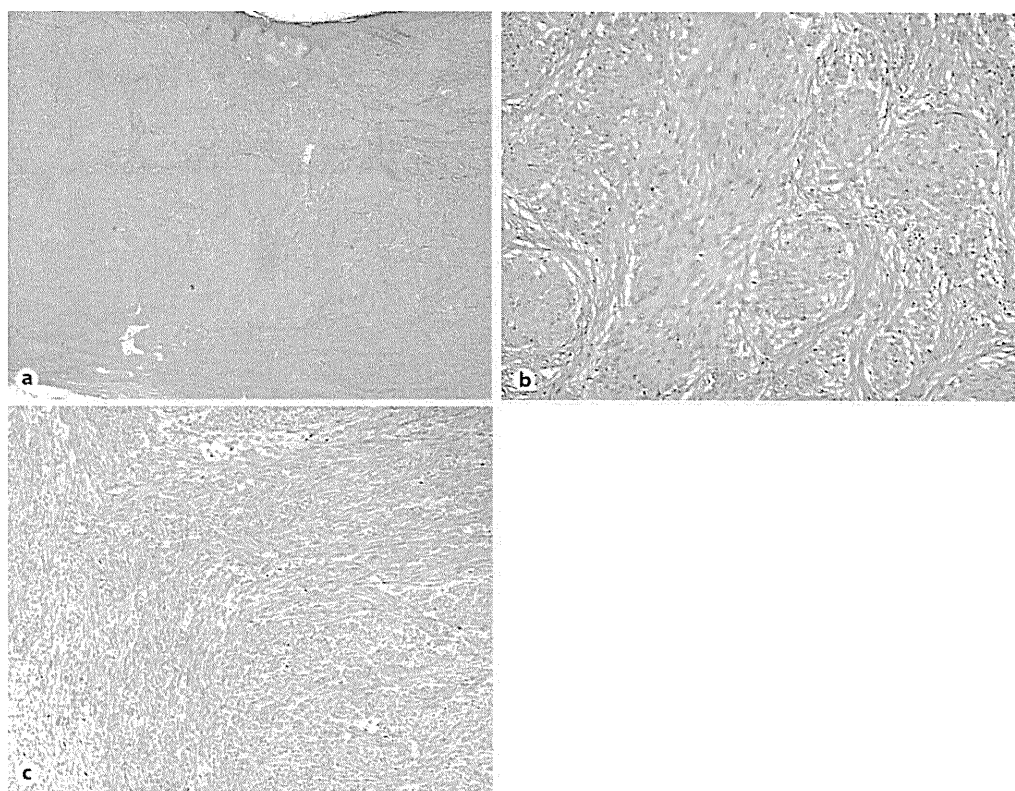

Fig. 1. Solid, red-colored subcutaneous nodule with a central concavity on the left shoulder.
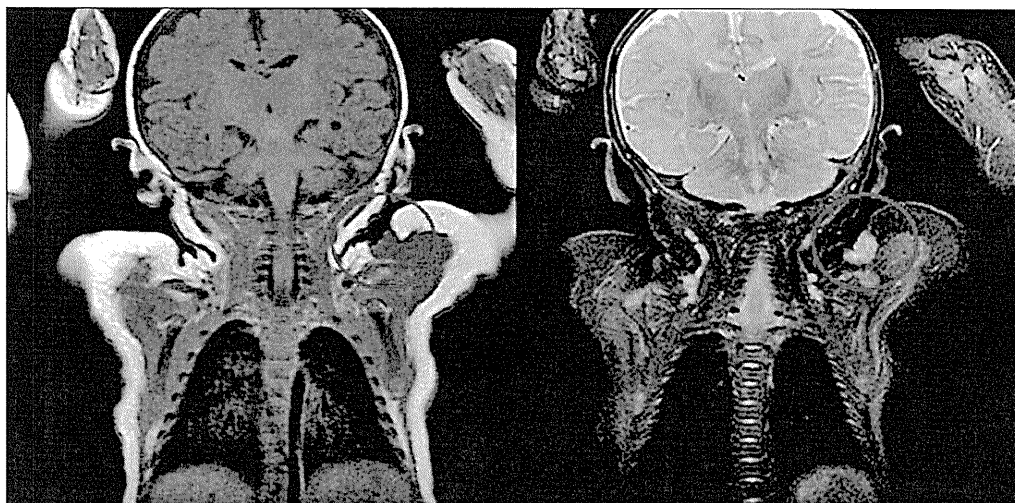
Fig. 2. MRI imaging showed the intensity of the nodule was similar to that of muscle. No additional lesions were found and infiltration of the tumor into the muscle was not observed.
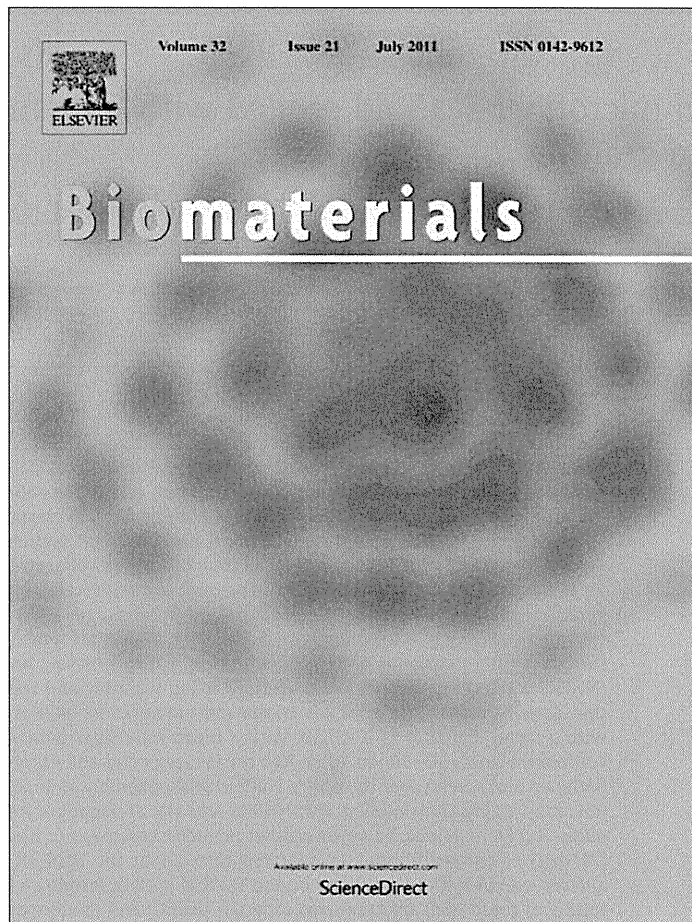

Fig. 3. Hematoxylin-eosin stain, original magnification ×20 (**a**), and ×100 (**b**). Specimen showed multifocal sclerotic dermal nodules composed of spindle cells and eosinophilic fibers. **c** Immunological staining of the tumor for α-smooth muscle actin (×100). Spindle cells express smooth muscle actin.

References

▶1   Stout AP: Juvenile fibromatosis. Cancer 1954;7:953–978.

▶2   Chung EB, Enzinger FM: Infantile myofibromatosis. Cancer 1981;48:1807–1818.

▶3   Larralde M, Hoffner MV, Boggio P, Abad ME, Luna PC, Correa N: Infantile myofibromatosis: report of nine patients. Pediatr Dermatol 2010;27:29–33.

▶4   Stanford D, Rogers M: Dermatological presentations of infantile myofibromatosis: a review of 27 cases. Australas J Dermatol 2000;41:156–161.

▶5   Goldberg NS, Bauer BS, Kraus H, Crussi FG, Esterly NB: Infantile myofibromatosis: a review of clinicopathology with perspectives on new treatment choices. Pediatr Dermatol 1988;5:37–46.

▶6   Hogan SF, Salassa JR: Recurrent adult myofibromatosis: a case report. Am J Clin Pathol 1992;97:810–814.

▶7   Wiswell TE, Sakas EL, Stephenson SR, Lesica JJ, Reddoch SR: Infantile myofibromatosis. Pediatrics 1985;76:981–984.

▶8   Ang P, Tay Y, Walford Y: Infantile myofibromatosis: a case report and review of the literature. Cutis 2004;73:229–231.

▶9   Dictor M, Elner A, Andersson T, Fernö M: Myofibromatosis-like hemangiopericytoma metastasizing as differentiated vascular smooth-muscle and myosarcoma. Am J Surg Pathol 1992;16:1239–1247.

▶10 Granter SR, Badizadegan K, Fletcher CD: Myofibromatosis in adults, glomangiopericytoma, and myopericytoma: a spectrum of tumors showing perivascular myoid differentiation. Am J Surg Pathol 1998;22:513–525.

11   Weedon D: Tumors and tumor-like proliferations; in Weedon D (ed): Skin Pathology, ed 2. Philadelphia, Churchill Livingstone, 2002, pp 767–768.

▶12 Variend S, Bax NMA, van Gorp J: Are infantile myofibromatosis, congenital fibrosarcoma and congenital hemangiopericytoma histogenetically related? Histopathology 1995;26:57–62.

▶13 Fields JP, Helwig EB: Leiomyosarcoma of the skin and subcutaneous tissue. Cancer 1981;47:156–169.

▶14 Staut AP, Hill WT: Leiomyosarcoma of the superficial soft tissues. Cancer 1958;11:844–854.

▶15 Toren A, Perlman M, Polak-Charcon S, Avigad I, Katz M, Kuint Y, Rechavi G: Congenital hemangiopericytoma/infantile myofibromatosis: radical surgery versus a conservative 'wait and see' approach. Pediatr Hematol Oncol 1997;14:387–393.

KARGER

A denatured collagen microfiber scaffold seeded with human fibroblasts and keratinocytes for skin grafting

Margit Kempf [a,1], Yuki Miyamura [b,1], Pei-Yun Liu [a], Alice C.-H. Chen [a], Hideki Nakamura [b], Hiroshi Shimizu [b], Yasuhiko Tabata [c], Roy M. Kimble [a], James R. McMillan [a,b,*,1]

[a] Centre for Children's Burns and Trauma Research (CCBTR), The University of Queensland, Queensland Children's Medical Research Institute, Brisbane, Australia
[b] Department of Dermatology, Hokkaido University Graduate School of Medicine, Sapporo, Japan
[c] Department of Biomaterials, Field of Tissue Engineering, Institute for Frontier Medical Sciences, Kyoto University, Japan

ARTICLE INFO

ABSTRACT

Biomaterial scaffolds are categorized into artificial or natural polymers, or combinations of the two. Artificial polymers often undergo serum protein adsorption, elicit foreign body and encapsulation immune responses post-implantation. Large pore bovine electrospun collagen I was therefore screened as a candidate for human keratinocyte and fibroblast cell scaffolds. Human HaCaT keratinocyte and dermal fibroblasts were seeded on electrospun denatured collagen I microfiber (DCM) scaffolds and after 72 h Livedead® assays performed to determine adhesive cell, survival and scaffold penetration. Both keratinocytes and fibroblasts attached to and survived on DCM scaffolds, however only fibroblasts migrated over and into this biomaterial. HaCaT keratinocytes remained largely stationary on the scaffold surface in discrete islands of monolayered cells. For this reason, normal human epidermal keratinocyte (NHEK) scaffold interactions were assessed using scanning and transmission electron microscopy (EM) that demonstrated DCM scaffolds comprised networks of interlocking and protruding collagen fibers with a mean diameter of 2–5 µm, with a mean inter-fiber pore size of 6.7 µm (range 3–10 µm) and scaffold thickness 50–70 µm. After 72 h the keratinocytes and fibroblasts on DCM scaffolds had attached, flattened and spread over the entire scaffold with assembly of lamellapodia and focal adhesion (FA)-like junctions. Using transmission EM, NHEKs and HaCaT keratinocytes assembled desmosomes, lamellapodia and FA junctions, however, neither hemidesmosomes nor basal lamina were present. In long term (21 day) co-culture fibroblasts migrated throughout the scaffold and primary keratinocytes (and to a lesser extend HaCaTs) stratified on the scaffold surface forming a human skin equivalent (HSE). In vivo testing of these HSEs on immunocompetent (BalbC) and immunodeficient (SCID) excisionally wounded model mice demonstrated scaffold wound biocompatibility and ability to deliver human cells after scaffold biodegradation.

1. Introduction

Skin tissue engineering addresses the need for early, permanent coverage of extensive skin injury in burns patients with an insufficient source of autologous skin for grafting [1,2]. Severe burn injuries require prompt wound closure but are hampered by limited patient donor site area and the high number of separate surgical operations often required to complete treatment [1,2]. In clinical situations in which insufficient donor skin is available, bioengineered skin in the form of cultured keratinocytes or in combination with fibroblasts to form human skin equivalents (HSEs) has allowed a greater expansion of donor surface area than conventional methods [3]. Cultured skin keratinocyte sheets are typically too fragile for transfer in vitro for engraftment and are commonly supported by biomaterial scaffolds that mimic specific tissues [4,5]. Such biomimetic scaffolds are classified into either naturally occurring [6–8] or artificial substrates [9] or combinations of the two source materials. We have previously tested artificial polymers that have many favorable properties [9], although

unfortunately some polymers have generally not performed up to expectations in the clinical setting [10–11]. Here, we examine the efficacy of a natural polymer scaffold derived from bovine collagen I. Previous biomimetic scaffolds have included freeze dried collagen sponges alone [4], sponges seeded with fibroblasts [12], collagen I scaffolds cross-linked with elastin [13], collagen II scaffolds [14], collagen and artificial polymer mixes [15–17], collagen cross-linked by carbodiimide [18] or electrospun collagen alone [19–21], electrospun collagen with epidermal keratinocytes [22] and scaffolds co-cultured with fibroblasts and keratinocytes [8,23]. The advantages of electrospun denatured collagen microfiber (DCM) scaffolds over frozen sponges come from a more homogenous pore structure and closer biomimetic structure to naturally occurring extracellular matrix [23] with pores of 5–10 microns allowing penetration of fibroblasts into the scaffold [24].

An important function of any potential skin substitute is to support the formation of a proper epidermal barrier to limit transepidermal water loss, infection and reduce the chances of hypertrophic scarring by speeding wound closure and ultimately patient recovery [25]. While the need to replace the epidermal barrier is paramount, restoration of normal structure and function of dermal tissue architecture is also critical to achieve acceptable cosmetic results [25]. Currently, there are very few skin substitutes that meet all of these criteria; however, recent cultured skin substitutes comprising fibroblast and keratinocyte cells on natural scaffolds meet many graft requirements [3,23]. The use of natural scaffolds patterned in novel ways to support reconstituted HSEs has primarily focused on reducing scar formation in animal wound models [8]. There are currently several animal wound models on which to test engraftment of human bioengineered skin composites onto immunodeficient mice to assess scarring [26]. In this study we have evaluated the use of DCM scaffold for supporting different human keratinocyte and fibroblast cell combinations for the preparation and transplantation of skin grafts from *in vitro* cultures. We have used *in vitro* cell viability assays to assess HaCaT keratinocyte and fibroblast cell attachment, survival, migration and morphology on DCM scaffolds. Due to the limitations of HaCaT cells to stratify in culture we also included primary human keratinocyte containing cultures in ultrastructural and functional HSE grafts studies. The biocompatibility of the DCM scaffold without cells was tested in excisionally wounded immunocompetent mice. In addition, the efficacy of different cell combinations of DCM composite grafts were tested in excisionally wounded immunocompromised SCID mice. Furthermore, the ability of the grafts to deliver live human cells and improve specific wound healing outcomes including reducing wound closure rates, shortening re-epithelialization times, reducing dermal foreign body and encapsulation immune responses and reducing dermal fibrosis was also assessed.

2. Materials and methods

2.1. Preparation of biomaterial

Denatured collagen microfiber (DCM) scaffolds were manufactured as previously described using acid extraction techniques [18] and subsequently disinfected/sterilized (using ethanol and UV light sterilization), washed, air dried and vacuum stored until required. Fiber diameter and morphology of the electrospun scaffold were controlled by concentration and molecular weight of the polymer as previously described [21,24,27]. Fiber diameters of 3–10 μm (greater than 3–4 μm) were produced to allow fibroblast cells to migrate into the scaffold [9]. Upon cell inoculation trapped air was removed using a combination of serial ethanol and sterile 0.1M Dulbecco's phosphate buffered saline (PBS) washes. This biomaterial was submersed in DMEM medium (Invitrogen, Gibco, BRL, Carlsbad CA, USA) before seeded with cultures of human fibroblasts or keratinocytes (HaCaT) keratinocyte cell line or primary normal human epidermal keratinocytes (NHEKs) or in combination. Sterilized, dehydrated DCM biomaterial was directly used for immunocompetent BalbC mouse biocompatibility experiments.

2.2. Cell sources

The cells (keratinocytes or fibroblasts) were only seeded on the upper DCM biomaterial surface. Fibroblast cells were sustained in Dulbecco's Modified Eagles Medium (DMEM) medium with 10% Fetal Calf Serum (FCS), penicillin and streptomycin (Gibco/Invitrogen, Mulgrave, Vic, Australia). HaCaT cells a gift from Dr. N. Fusening (German Cancer Research Center, Heidelberg, Germany) [28] were also maintained in DMEM medium (Gibco/Invitrogen, Mulgrave, Vic, Australia). Normal human neonatal foreskin keratinocytes (Cambrex, Walkersville, MD, catalogue number CC-2503) were grown or isolated in KGM I culture medium (Clonetics, MD/Cambrex, Walkersville, MD, USA) until passage 2 or 3 (P2/P3). Alternatively, primary keratinocytes obtained from surgical specimens (with institutional ethical approval) were maintained in SFM medium (Gibco/Invitrogen, Mulgrave, Vic, Australia) and supplemented with EGF and BPE growth factor supplements (as per the manufacturer's instructions). The cells were then trypsinized and stored in 10% DMSO under liquid nitrogen until required. Normal human dermal fibroblasts were obtained from surgical specimens or commercially (Cambrex, Walkersville, MD, catalogue number 1/2F0-C25) and grown in DMEM with 10% FCS (Cambrex, Walkersville, MD) until passage 5 (P5). Cells were then trypsinized and stored in 10% DMSO under liquid nitrogen until required.

To create primary keratinocyte-fibroblast composites that have the ability to form a stratified epidermis in culture, $1 \times 10^5/cm^2$ fibroblasts were seeded onto a DMEM medium pre-soaked DCM scaffold at day 0 (seeded cells were maintained in place on the DCM by a modified pipette tip used as an insert). From day 1 these cells were maintained in UCMC 160 medium [29] as previously described [23]. Concurrent with fibroblast confluence on the DCM on day 5, $1 \times 10^6/cm^2$ keratinocytes were directly seeded in UCMC 160 medium onto the scaffold composites to create a bilayered composite (again, using the modified pipette tip as a retainer). At day 6 the insert was removed and the composite was placed into 6 well plates and transferred onto a nylon mesh platform (Mersilene™ Polyester Fiber Mesh, Ethicon, Johnson and Johnson, Langhorne, PA) to maintain it at the air–liquid interface. From day 10 onwards neither progesterone nor EGF growth factors (supplied with UCMC 160 medium) were added to the UCMC 160 medium. Composites were maintained in UCMC 160 until day 26 with a culture medium change at least every 48 h.

2.3. Livedead® cell survival assay

Low passage, HaCaT keratinocytes (<P10) or dermal fibroblasts (<P5) were expanded and maintained in the previously described DMEM culture medium. Cells were trypsinized, counted and 3.5×10^5 cells per cm² plated onto pre-prepared DCM substrate. This density has previously been determined to be sufficient for proper seeding of keratinocytes onto grafts [9,30]. Cells were stringently washed 4 times in sterile 0.1M Dulbecco's phosphate buffered saline to removed non-adherent cells and maintained for 72 h on DCM biomaterial. After 72 h, the cell-biomaterial composites were then subjected to the Livedead® fluorescence assay according to the manufacturer's instructions and the numbers of live (green) non-viable/dead (red) cells (either HaCaT keratinocytes or fibroblasts) immediately assessed using an Olympus Fluoview FV300 confocal and IX70 inverted microscope (Olympus, Tokyo, Japan) with a ×20 objective lens. Only attached, live, uniformly green fluorescent cells or typically small, pyknotic red cells were counted. The mean percentage of live (green florescent) and pyknotic red (dead) cells were calculated (from $n = 3$ microscope fields of view repeated three times) as a fraction of total cell numbers represented by the presence of counterstained cell nuclei. Statistical analysis was performed between identical control cells grown on tissue culture plastic (TCP) the treatment groups using one way measure of variance and two sample *t*-tests using the Minitab statistical package (Minitab Incorporated, University of Pennsylvania, Philadelphia, PA, USA) at a p value <0.05 or <0.01 showing significant effects.

2.4. Scanning electron microscopy

DCM substrate alone or monocultures of cells on DCM substrate (fibroblasts, HaCaTs or primary keratinocyte) were maintained for 72 h and subsequently fixed in 2% glutaraldehyde for at least 4 h and processed for routine scanning electron microscopy (SEM) as previously described [9]. Briefly, samples were dehydrated in a graded ethanol series, treated twice with isoamyl acetate, critical point CO_2 dried using a Hitachi HCP-2 (Hitachi, Tokyo, Japan) followed by optional platinum-palladium sputter coating in a Hitachi E–1030 (Hitachi, Tokyo, Japan). Specimens were examined using either a Hitachi S-4500 or JEOL 6400F SEM microscope fitted with a digital image capture system (Japan Electron Optical Ltd, Tokyo, Japan). Over 100 surface adherent cells were examined as a representative sample per cell type on the DCM substrate.

2.5. Transmission electron microscopy

Cell monocultures (keratinocytes or fibroblasts) were maintained on films for over 72 h (between 3 and 26 days) and were fixed in 2% glutaraldehyde solution, post-fixed in 1% OsO_4, dehydrated, and processed for conventional electron microscopic observation according to the methods described by [9]. Semithin sections were cut and stained with Richardson's stain and mounted using cyanoacrylate glue [31,32].

HaCaTKeratinocytes DCM (day3)   Dermal fibroblasts (day3)   HaCaTKeratinocytes TCP (day3)
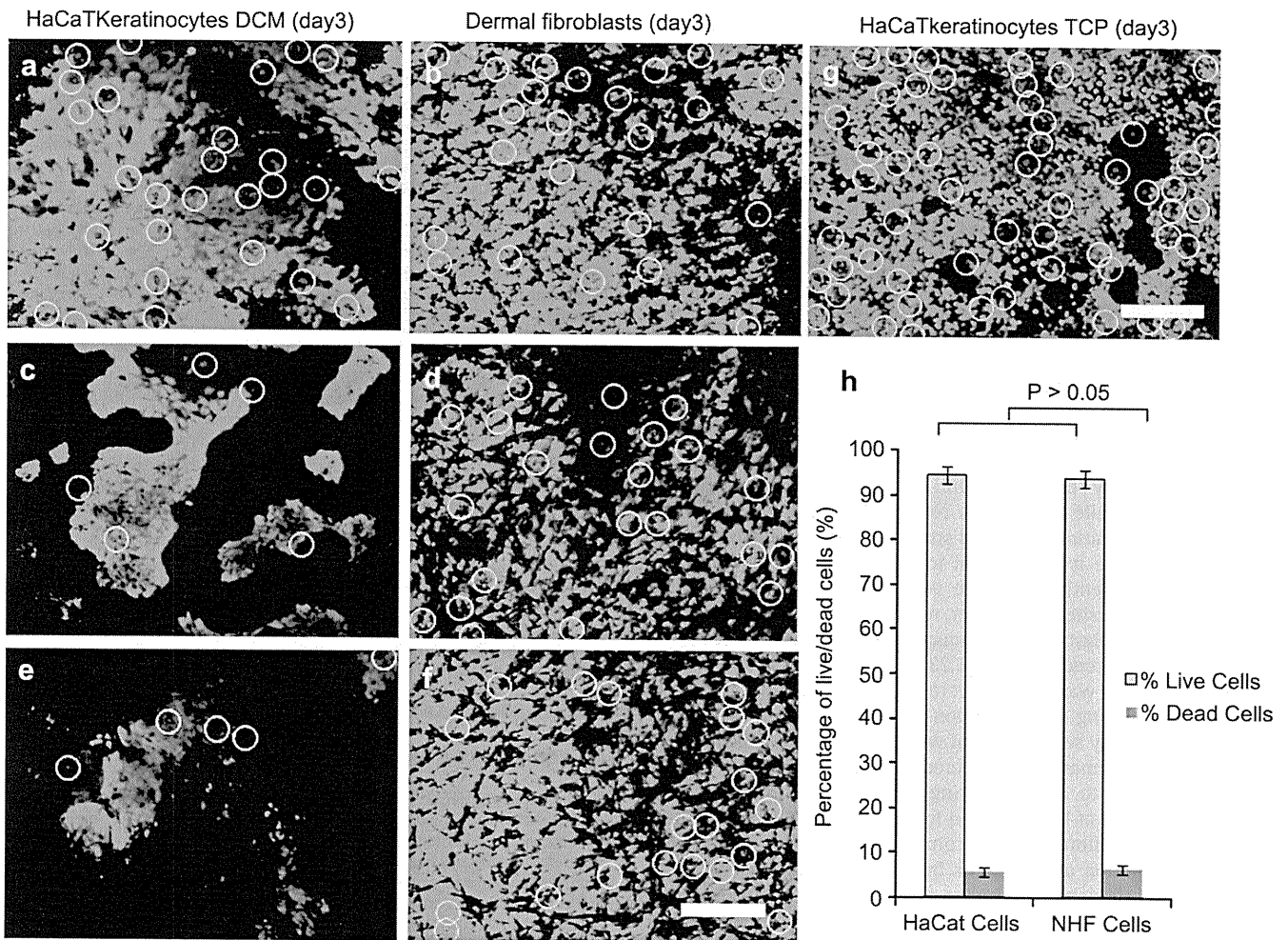
Fig. 1. Both HaCaT keratinocytes (a, c, e) and normal human dermal fibroblasts (b, d, f) exhibited variable cell densities on the same denatured collagen microfiber (DCM) and could adhere and survive under standard cell culture conditions. HaCaT keratinocytes (green cell in a, c, e) exhibited variable-sized islands of cultured cells with very little evidence of cell migration over or penetration into the core of the of DCM biomaterial fibers. Small numbers of individual dead keratinocyte or fibroblasts were apparent (highlighted by white circles over dead cells stained red in a–g). Conversely, fibroblasts demonstrated evidence of cell spreading and migration over and penetration within the entire DCM biomaterial (as highlighted by live cell confocal green fluorescent signal being interrupted by non-fluorescent DCM fibers in b, d, f). This is in contrast to uninterrupted staining of cells (HaCaT or fibroblasts, g) maintained on tissue culture plastic (TCP). Scale bar 200 μm. Image analysis of these images produced estimates of over 94% cell viability (and around 5% non viable cells) for both cell types maintained on DCM biomaterial (HaCaTs 94.3%, fibroblasts 93.6% viable). (For interpretation of the references to colour in this figure legend, the reader is referred to the web version of this article).

Samples were cut, stained with uranyl acetate and lead citrate and viewed under a JEOL 1010 transmission electron microscope at 75–80 kV with digital image capture.

2.6. Assessment of DCM biomaterial wound biocompatibility in immunocompetent mice

These two procedures, experiments 1 and 2 were performed based on a previous protocol [33]. All animal procedures were conducted according to guidelines provided by the appropriate University Biomedical Institutional Animal Ethics Committee under an approved protocol governing the use of experimental animals. For experiment 1, DCM biomaterial was grafted onto two groups ($n = 5$ each) of 6 week old BALB/cA Jcl immunocompetent mice to assess the effect of the DCM scaffold on excisional wounding without the presence of any human cells (DCM treated or control untreated). The mice were anesthetized with a intra peritoneal (i.p.) injection of 50 mg/kg Ketamine/10 mg/kg Xylasil with additional top-up iso-fluorane anesthetic as required (0.5–2% isofluorane flow rate of O_2 at 0.5–0.75L/min). The dorsal fur was clipped, ethanol cleaned and a 4 mm diameter full-thick-ness excisional punch biopsy (Provet, Pty Ltd, Australia) wound made through the back skin. A 4 mm punch biopsy disc of DCM biomaterial was placed and secured within the boundary of original excisional wound or left untreated as a control. All the wounds were then immediately dressed with occlusive film (GLAD Wrap ©, Padstow, NSW Australia) to maintain the wound in a moist environment and held in place for 1 week by Fixomull bandage (Smith and Nephew Healthcare, Hull, UK). After 7 days the dressings were removed and the dimensions of each wound were

then digitally photographed and recorded on a daily basis and wound closure rates assessed using image analysis software (Image Pro Plus V9, Media Cybernetics, Bethesda, MD, USA). Wound closure was defined as the point when the epidermal skin surface appeared completely re-epithelialized (closed) with no evidence of underlying tissue such as bodily secretions, exudate or crusted blood. Wound size and closure rates were calculated by converted pixel area to wound area in mm^2 until complete re-epithelialization had taken place (performed in a standardized fashion by one individual). All wounds were repaired within 18 days. After 21 days the mice were sacrificed by CO_2 asphyxiation and the remaining dorsal skin shaved. The centre of each wound was then labeled with indelible (permanent) marker and the biopsy excised with a 20–50 mm border of normal skin (for orientation purposes) processed for histological examination.

2.7. Assessment of DCM cell composites on wound healing in immunosuppressed mice

In mouse experiment 2, we assessed the effects of different combinations of cell-DCM biomaterial composites in our excisionally wounded SCID (C.B-17 Icr-Scid Jcl strain on a BALB/c background) model mice using five groups of 6 week old immunodeficient mice ($n = 5$ per group, 35 in total) were included in this experiment. The mice were prepared and treated as previously described but each group was treated with a different biomaterial composite wound insert. The groups comprised 1) wounded untreated mice, 2) wounded/DCM/nylon nylon Mersilene™ nylon mesh support(mesh) treated mice, 3) wounded/mesh support alone treated
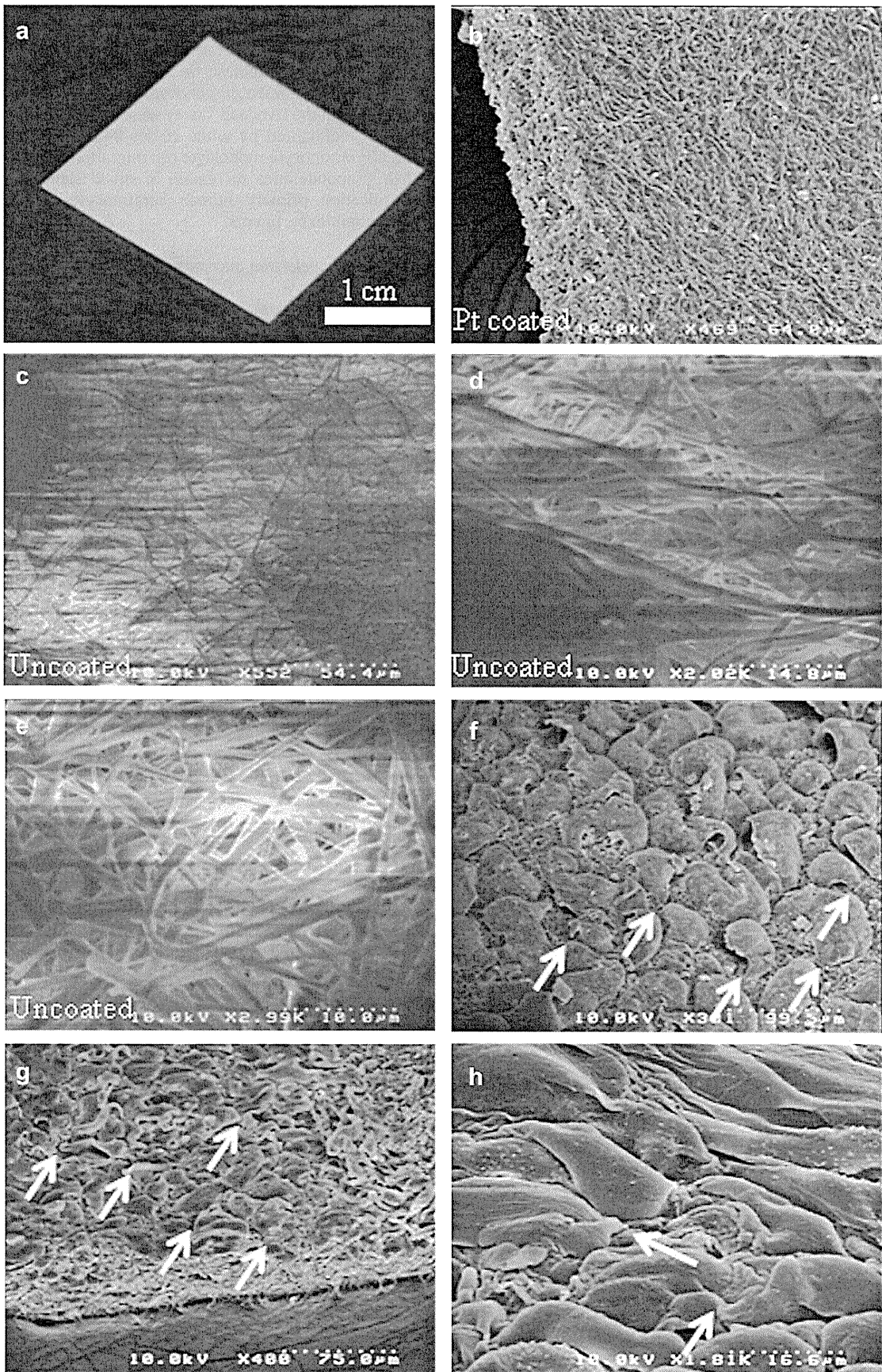
mice and 4) wounded/DCM/mesh/HaCaT/fibroblast and 5) wounded/DCM/mesh/NHEK/fibroblast human skin equivalent treated SCID mice (see previous methods section for details of cell-DCM biomaterial culture). Wounds were dressed for 1 week only and wound closure assessment made from day 7 until complete re-epithelialization. Macroscopic wound photographic results from individual animals and averaged group results of closure rates and total time to wound closure from each treatment group of animals were assessed using image analysis software (Image Pro Plus V9, Media Cybernetics, Bethesda, MD, USA) and displayed graphically. All mice were sacrificed on day 21 and wound biopsies taken for histological assessment as described below.

2.8. Immunohistological wound assessment

Fur-clipped, indelibly marked wounded mouse skin and surrounding, perilesional unwounded skin were removed and either embedded in OCT compound (SAKURA, Torrance, CA) to be snap frozen in liquid nitrogen cooled isopentane or fixed in 4% formaldehyde in phosphate buffered saline, and processed for paraffin embedding for routine H&E and modified Masson's Trichrome stains for histological analysis (to assess wound healing responses, fibrosis and identify areas of neodermis containing newly synthesized collagen). Wounds were assessed by multiple serial sectioning and selection of tissue from the closest point to the center of the wound.

To assess the persistence and migration of human cells delivered into mouse wound tissue from the biomaterial graft in the SCID mouse model we performed indirect immunofluorescence using frozen, unfixed cryostat sections of mouse wounded skin treated with cell-biomaterial composites and normal human skin sections as controls. Briefly, cryostat tissue sections were fixed in acetone and incubated with primary antibody/antisera. Sections were incubated with secondary antibodies conjugated to fluorescein isothiocyanate (FITC; rabbit anti-mouse IgG or goat anti rabbit IgG; 1: 200; Dako, Tokyo, Japan). Sections were then labeled with a 4',6-diamidino-2-phenylindole (DAPI) nuclear counter stain contained in Vectashield mounting medium (Vectorlabs, Burlingame, CA, USA). The sections were examined with an Olympus Fluoview FV300 confocal microscope (Olympus, Tokyo, Japan) in duplicate. Controls included human skin cryostat sections with the primary antibody substituted by PBS, myeloma supernatant or an irrelevant immunoglobulin isotype, as a negative control. All experiments were performed in duplicate.

2.9. Statistical analysis

For quantitative measurements either the Student's t-test for two sample comparison or for multiple comparison ANOVA was performed (Minitab Incorporated, University of Pennsylvania, Philadelphia, PA, USA) at a P value < 0.05 or < 0.01 to demonstrate significance.

3. Results

3.1. Livedead® cell assay

The results show that DCM scaffold is able to maintain adhesion and cell survival of both keratinocyte HaCaT cells (Fig. 1a, c, e) and fibroblasts on DCM (Fig. 1b, d, f) in a similarly effective fashion as cells cultured on conventional tissue culture plastic (TCP) (g). There were however, two main differences between keratinocyte and fibroblast migration on DCM compared to TCP. Firstly, keratinocyte cells formed discrete islands over a limited area on the DCM surface suggesting that lateral migration over the surface of DCM is severely limited or completely inhibited compared to fibroblasts (Fig. 1a, c, e versus b, d, and f). Secondly, migration of the primary human fibroblasts into the DCM matrix was much more evident as demonstrated by the pattern of dark 2-5 μm-thick fibers crossing the images obscuring the live (green fluorescent) cells in the center of the DCM biomaterial (Fig. 1b, d, f) compared to the unobscured

keratinocytes (Fig. 1a, c, e). For each cell type the percentage of viable cells (in green) was very high and ranged between (94–96% viability) with HaCaT keratinocyte cells demonstrating a similar mean viability to fibroblasts on DCM (Fig. 1h $p > 0.05$) or compared to HaCaTs maintained on polystyrene TCP (96.2% live see Fig. 1g). Dead cells in the Livedead® assay were shown as small dots stained in red (highlighted by white circles a–g). Due to limitations in HaCaT keratinocyte monolayer cell migration over DCM (shown by their preponderance to remain in small islands) and to induce stratification primary human keratinocytes were included in subsequent experiments.

3.2. Scanning electron microscopy

Gross macroscopic analysis of the DCM biomaterial demonstrated a thin, moderately stiff white, paper-like fibrous biomaterial (Fig. 2a) that became softer and more pliable upon immersion in aqueous solutions. Low power scanning electron microscopy (SEM) of platinum coated samples revealed a complex multilayered fibrous structure comprising a compact network of randomly oriented (non-woven) fibers of various thicknesses ranging in diameter from 2 to 5 μm (mean diameter of 4.3 μm, $n = 50$ fibers) and with variable inter-fiber porosity ranging between 3 and 10 μm (mean 6.7 μm, $n = 50$ fibers). This considerable range in DCM fiber diameter (up to 2.5 fold) coupled with variable porosity are crucial design characteristics of this biomaterial [9,24]. Overall the entire thickness of the DCM biomaterial ranged between 50 and 70 μm (Fig. 2b) and visualization into the upper 10–20 μm layers of fibers of this fibrous sheet was possible in uncoated samples (i.e. without Pt coating, Fig. 2c–e). DCM cell composites demonstrated normal primary human epidermal keratinocyte (NHEK)(Fig. 2f), HaCaT keratinocyte cell line (Fig. 2g) and fibroblast cell (Fig. 2h) attachment and spreading on the fibrous biomaterial surface. Cell membrane processes involved the formation of lamellapodia and putative sites of focal contact formation were observed (see white arrows in Fig. 2f–h).

3.3. Transmission electron microscopy

Semithin sections of normal human skin demonstrated multilayered, keratinizing epidermal layers and bundles of well organized collagen fibers in the dermis (labeled D in Fig. 3a). Plastic embedded, sectioned biomaterial (Fig. 3b) and skin cell-biomaterial composites (Fig. 3c–g) demonstrated that DCM is a good dermal substitute allowing keratinocyte and fibroblast cell adhesion/survival and fibroblast migration over and penetration into the DCM biomaterial. DCM comprised a more amorphous aggregation of randomly distributed and oriented electrospun fibers (Fig. 3b). Despite this, normal primary human epidermal keratinocytes (NHEK) (Fig. 3c), HaCaT keratinocyte cells (Fig. 3d) and normal fibroblasts (Fig. 3e) all adhered directly on to the DCM scaffold. Furthermore, fibroblasts migrated into the DCM when cultured either alone or co-cultured with HaCaT keratinocyte cells (Fig. 3e and f). Co-cultures of HaCaT and fibroblasts on DCM (Fig. 3f), however, failed to form a multilayered, well stratified and keratinized epidermal layer, despite the


Fig. 2. Macroscopic and electron microscopic views of denatured collagen microfiber (DCM) biomaterial without seeded cells (a–e) and with seeded skin cells (keratinocytes f, g and fibroblasts h). Macroscopic view of DCM biomaterial reveals a variably stiff but thin white fibrous material resembling a good quality slightly thickened paper sheet that becomes soft and flexible when hydrated (a). Scanning electron microscopy (SEM) of Pt coated DCM shows a dense network of randomly interwoven fibers with a well defined, almost solid surface that upon closer SEM inspection of uncoated samples (hence the DCM biomaterial exhibited some static charging effects) revealed a network of large pores (between 3 and 10 μm mean 6.7 μm) and channels between loose, randomly oriented electrospun DCM fibers 2–5 μm in thickness (c–e) with a mean fiber diameter of 4.3 μm. HaCaT and primary keratinocytes (f and g) and fibroblasts (h) were seeded on DCM and maintained in culture for between 3 and 8 days. Keratinocytes formed small rounded, dome shaped cells with cytoplasmic focal contact projections resembling lamellapodia extending toward the DCM surface. Fibroblasts however, formed longer, thinner elongated cells with fewer, typically 3–4 focal contact like projections at the ends of lamellapodia. Several small sections of fibroblasts were observed protruding from within the DCM channels and pores (data not shown).
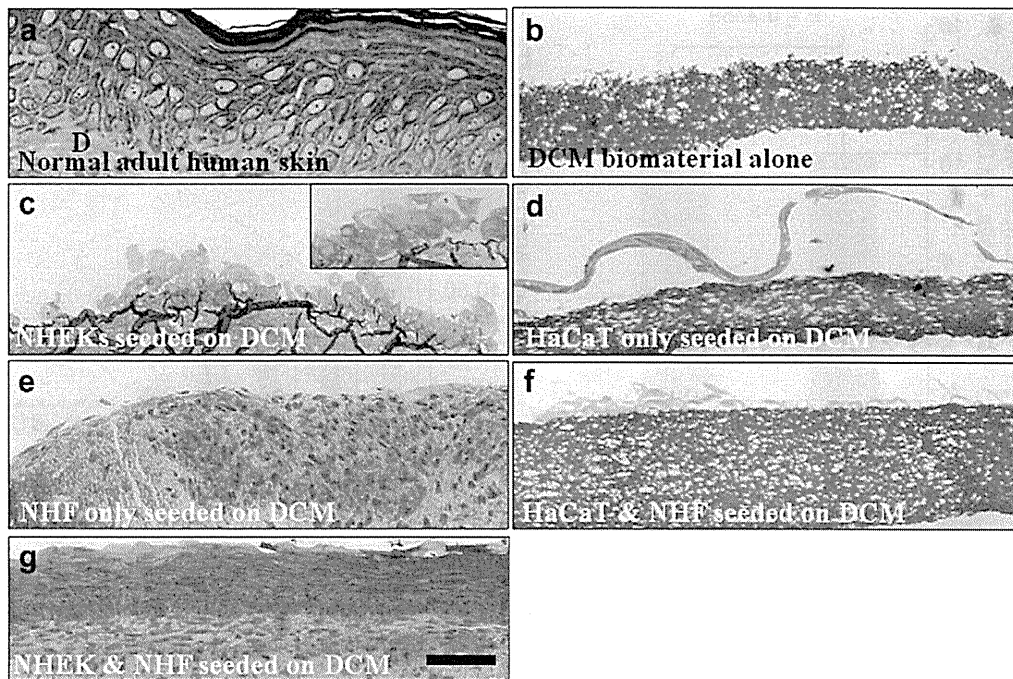
Fig. 3. Semithin plastic embedded sections show normal human skin (a) with stratified, keratinized epidermal layers over lying bundles of dermal collagen (labeled as D in a), whereas the structure of DCM scaffold (b) is more amorphous and significantly thinner than human dermal tissue with a thickness of between 50 and 70 μm. Cell-biomaterial composites show that primary keratinocytes (c) HaCaT cells (d)/and fibroblasts (e) adhere to DCM scaffolds (b) and can be maintained in culture. Seeded primary (c) and HaCaT (d) keratinocyte monocultures adhere to DCM with the formation of thin multilayered epidermal keratinocytes in culture. Fibroblasts, however, proliferate (more than any of the keratinocyte cell types) over the surface of the DCM and in addition penetrate the porous DCM fibers in culture (e). co-culture of HaCaT and fibroblast cells led to a loss of epidermal architecture and increases in HaCaT/fibroblast-DCM penetration (f). Conversely, co-culture of primary NHEKs and fibroblasts on DCM over 26 days at the air liquid interface (g) demonstrated remarkable levels of epidermal stratification and differentiation in addition to fibroblast invasion into the DCM substrate. Scale bar 150 μm. (For interpretation of the references to colour in this figure legend, the reader is referred to the web version of this article).
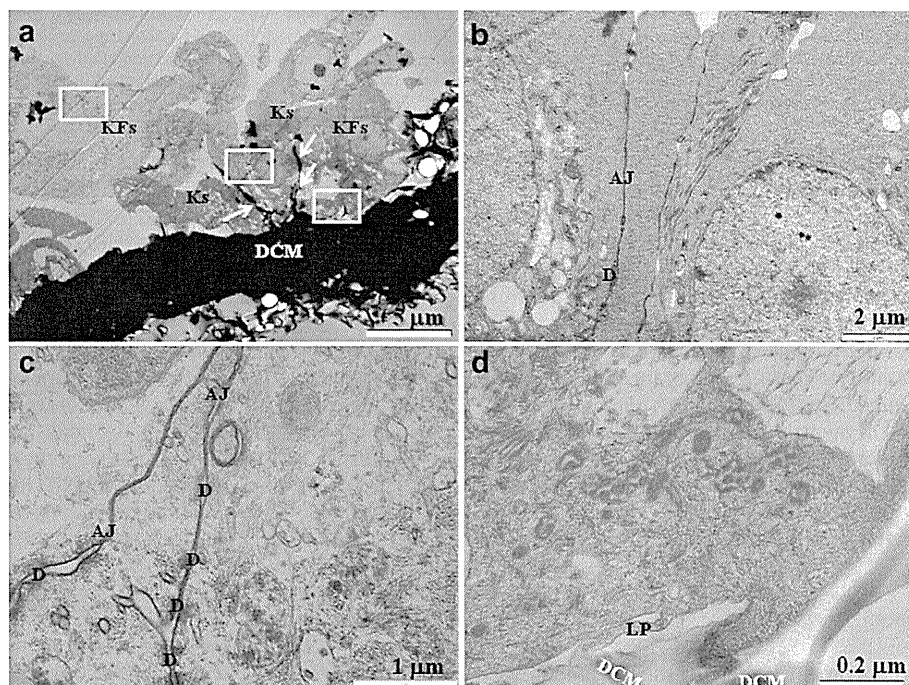
Fig. 4. Ultrastructural examination of primary human keratinocytes seeded on DCM showed a multilayered keratinocyte cell sheet attached to an electron dense DCM scaffold. Thin electron dense DCM fiber projections (white arrows in a) were noted between basal keratinocyte cells (Ks) close to the DCM scaffold (DCM). (b) In areas of close keratinocyte cell apposition highlighted by the middle white box in (a) there were cell–cell desmosomal junctions (labeled D) and adherens junctions (AJ). In areas these structures were quite numerous (left hand box in a, shown in c). However, in areas of keratinocyte-DCM apposition (right hand white box in a, shown in d) there were no signs of any hemidesmosomes linking the DCM substratum (d) only lamellapodia (LP) with putative focal contact like junctions.
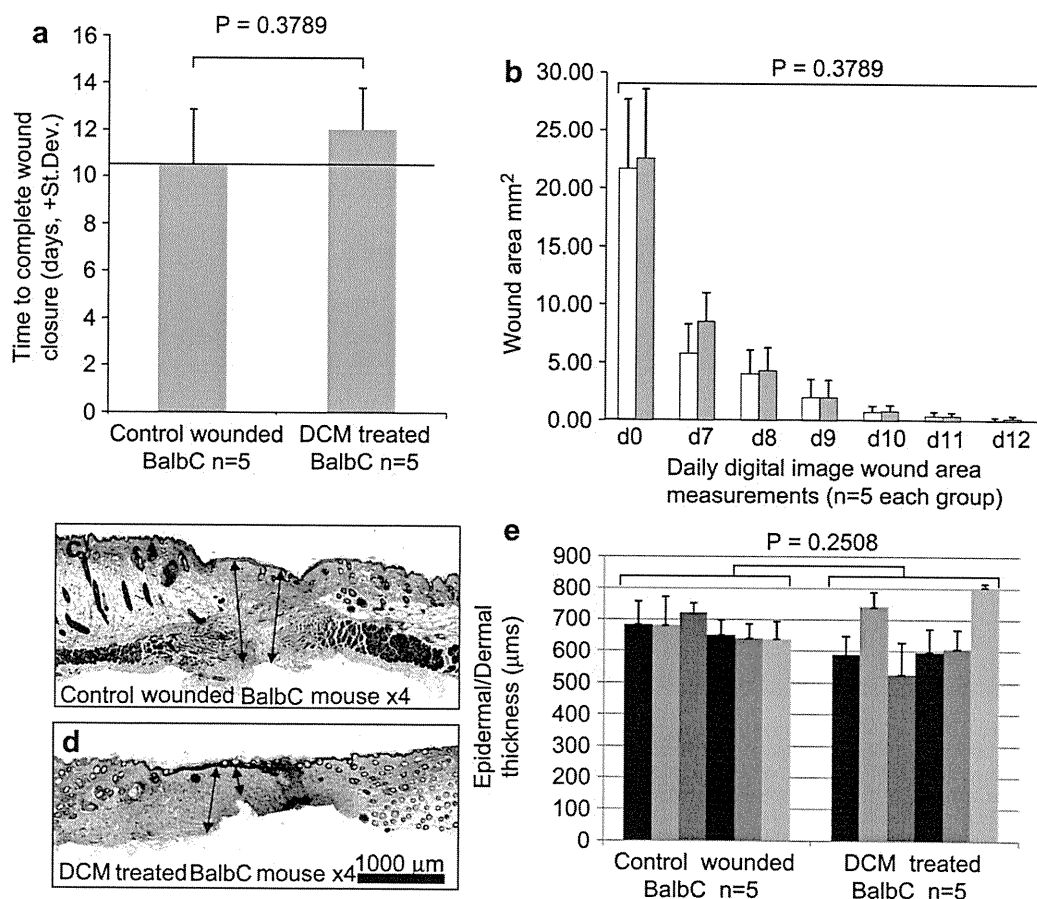
Fig. 5. Excisionally wounded immunocompetent BalbC model mice showed no difference in mean time to complete wound closure (a) or in the mean rate of wound closure (b) with or without DCM scaffold wound treatment ($n = 5$ each group). Furthermore, the effect of DCM scaffold incorporation into the healing excisional wound failed to induce significant foreign body wound immunoreactivity or scarring response as demonstrated by increases in the mean thickness of either wounded epidermal or dermal tissue (new collagen deposition stains blue see arrows in c and d) in modified Masson's Trichrome stained paraffin embedded mouse skin sections. Individual wound thickness measurements for each of the 5 BalbC mice per group demonstrated no alterations in wound thickness between treatment groups ($p > 0.251$). (For interpretation of the references to colour in this figure legend, the reader is referred to the web version of this article).

composite being raised to air–liquid interface on mesh supports and the DCM scaffold acting as a dermal substitute for fibroblast invasion. Conversely, co-culture of fibroblast and NHEK cells produced, 4–5 cell multilayered, polarized, well stratified and partially keratinized epidermal-like continuous structure (Fig. 3g). Ultrastructurally, the NHEK keratinocytes on the DCM exhibit good close cell–cell association with the presence of perinuclear keratin filaments (KFs, Fig. 4a) that upon higher magnification reveal closely apposing adjacent keratinocyte plasma membranes (Fig. 4b) with both desmosomal (D) and adherens junction (AJ) like structures on the membrane (Fig. 4c). On the basal border of the basal layer keratinocyte over lying the biomaterial (labeled DCM in Fig. 4d)there is a marked absence of hemidesmosomal cell-matrix junctions but instead there is are small membrane like lamellapodia-like processes consistent with the presence of focal contract cell-matrix junctions (LP in Fig. 4d).

3.4. Wounded model mice

Our data show from experiment 1 assessing the biocompatibility of DCM in BalbC mice demonstrated the incorporation of DCM scaffold without cells into wounded mouse tissue on immunocompetent mice has little or no adverse effect on the processes of normal wound healing and subsequent wound closure times in all 5 mice tested in each treatment group (Fig. 5a, $p > 0.05$) and rates of wound closure

(Fig. 5b, $p > 0.05$). There was little difference in wound appearance between each of the different treatment groups with the main difference being slight changes in the rate of wound healing.

Both hematoxylin and eosin (H&E, data not shown) and modified Masson's Trichrome stained paraffin sections of mouse skin (Fig. 5c and d) showed similar re-epithelialization rates (Fig. 5a and b) and levels of skin thickening, 21 days after excisional wounding in both untreated and DCM treated mouse groups (Fig. 5e). Furthermore, there was no statistical difference in combined mean epidermal and dermal wound thickness (suggestive of scarring likelihood) over the excisional wounds themselves at 21 days post wounding (Fig. 5e).

Similarly, in experiment 2 assessing the efficacy of combinations of cell-DCM-scaffold composites in SCID mice there was no difference in mean would closure times (Fig. 6b, $p > 0.05$) or wound closure rates (Fig. 8) between the 5 treatment groups seeded with or without combinations of human fibroblast and keratinocyte-DCM grafts in our SCID mouse animal model. Normal human skin was used as the positive control from anti-human HLA staining (see asterisks in Fig. 7a) for human cells in mouse wounds. Confocal microscopy using anti-human HLA antibody staining of wounded mouse skin after treatment with 2 of the 5 graft combinations including human cells on DCM scaffold demonstrated that these cells were engrafted into the wounded mouse tissue, survive and were maintained there for up to 21 days post injury (see asterisks in Fig. 7e and f verses Fig. 7b–d).